Fundamental Equation of State for Deuterium

I. A. Richardson, J. W. Leachman, and E. W. Lemmon

Citation: Journal of Physical and Chemical Reference Data **43**, 013103 (2014); doi: 10.1063/1.4864752
View online: https://doi.org/10.1063/1.4864752
View Table of Contents: http://aip.scitation.org/toc/jpr/43/1
Published by the American Institute of Physics

Fundamental Equation of State for Deuterium

I. A. Richardson and J. W. Leachman [a)]

HYdrogen Properties for Energy Research (HYPER) Laboratory, School of Mechanical and Materials Engineering, Washington State University, P.O. Box 642920, Pullman, Washington 99164, USA

E. W. Lemmon

Applied Chemicals and Materials Division, National Institute of Standards and Technology, 325 Broadway, Boulder, Colorado 80305, USA

(Received 30 September 2013; accepted 27 January 2014; published online 27 February 2014)

World utilization of deuterium is anticipated to increase with the rise of fusion-energy machines such as ITER and NIF. We present a new fundamental equation of state for the thermodynamic properties of fluid deuterium. Differences between thermodynamic properties of orthodeuterium, normal deuterium, and paradeuterium are described. Separate ideal-gas functions were fitted for these separable forms together with a single real-fluid residual function. The equation of state is valid from the melting line to a maximum pressure of 2000 MPa and an upper temperature limit of 600 K, corresponding to available experimental measurements. The uncertainty in predicted density is 0.5% over the valid temperature range and pressures up to 300 MPa. The uncertainties of vapor pressures and saturated liquid densities are 2% and 3%, respectively, while speed-of-sound values are accurate to within 1% in the liquid phase. [http://dx.doi.org/10.1063/1.4864752]

Key words: deuterium; equation of state; normal deuterium; orthodeuterium; paradeuterium; thermodynamic properties.

CONTENTS

List of Tables

[a)]Author to whom correspondence should be addressed; electronic mail: jacob.leachman@wsu.edu.

List of Figures

1. List of Symbols

a	Helmholtz free energy, J/mol
B	second virial coefficient, cm^3/mol
C	third virial coefficient, cm^6/mol^2
c_p	isobaric heat capacity, J/(mol K)
c_v	isochoric heat capacity, J/(mol K)
h	enthalpy, J/mol
p	pressure, MPa
R	molar gas constant, 8.3144621 J/(mol K)
s	entropy, J/(mol K)
T	temperature, K
w	speed of sound, m/s
Z	compressibility factor, $p/\rho RT$
α	reduced Helmholtz energy
δ	reduced density
ρ	molar density, mol/dm^3
τ	inverse reduced temperature

Subscripts

c	critical-point property
r	reduced property
σ	saturation property
0	reference property

Superscripts

r	real-fluid property
0	ideal-gas property

2. Introduction

The rising costs and environmental impact of using fossil fuels for power production are increasing the desirability of nuclear energy. Nuclear fusion reactors such as ITER and the National Ignition Facility (NIF) are under development to use large amounts of the hydrogen isotope deuterium (D_2) as fuel. The increasing demand for deuterium as a nuclear fuel and as a stable isotopic tracer ensures the continued demand of deuterium for decades to come.

A recent examination of the thermophysical properties of deuterium conducted by Richardson and Leachman[1] established the need for a new Equation of State (EOS). This paper describes new equations for normal deuterium (nD_2), orthodeuterium (oD_2), and paradeuterium (pD_2) that have been developed to replace the previous existing EOS for deuterium. The existing deuterium model currently in use by the National Institute of Standards and Technology's (NIST) standard properties package, REFPROP,[2] was developed by McCarty[3] in 1989. Though there have been no new experimental measurements since the development of McCarty's equation, the computing capabilities, fitting techniques, and functional forms of modern EOS have significantly improved. The McCarty EOS also did not consider the effects of the spin isomers that exist for deuterium that influence properties such as ideal-gas heat capacities by as much as 30%.[4] The deuterium model developed by McCarty is based on the International Practical Temperature Scale of 1968 and has upper pressure and temperature limits of 320 MPa and 423 K.

The new nD_2, oD_2, and pD_2 equations of state are explicit in reduced Helmholtz free energy and are similar to the equations for light hydrogen described by Leachman *et al.*[5] The equations of state for the various spin isomers of deuterium share the same 21-term real-fluid residual equation. To account for significant differences in ideal-gas behavior, each of the three equations of state for deuterium has a unique ideal-gas equation. The differences among nD_2, oD_2, and pD_2 will be discussed in greater detail below. The EOS developed in this work extends the range of reliable property predictions to 2000 MPa and 600 K, and extrapolates to 2000 K without obvious deviations from accepted theories on thermophysical property behavior.

3. Nuclear Spin Isomers of Deuterium

Similar to the hydrogen molecule, deuterium molecules have separable nuclear spin isomers denoted as "ortho" and "para." A detailed discussion of the historical significance of these forms can be found in Leachman *et al.*[5] In short, spin isomers exist in the deuterium molecule due to the parity between the nuclear spin function and rotational spin function. For simple, isotopic diatomic molecules, the rotational spin, J, of the two nuclei can either be symmetric ($J = 0, 2, 4, \ldots$) or antisymmetric ($J = 1, 3, 5, \ldots$). As deuterium cools to cryogenic temperatures, insufficient energy is available to populate higher-energy modes. Approaching absolute zero, molecules in the even J states de-excite to $J = 0$, while molecules in the odd J states de-excite to $J = 1$. Deuterium molecules below 50 K in the $J = 1$ rotational state are metastable and may take days or weeks to de-excite to the $J = 0$ rotational state in the absence of a suitable catalyst. This parity allows for two separable and interconvertible deuterium forms.

Contrary to hydrogen and tritium, the lower-energy, even-J states are denoted "ortho" for deuterium, while the higher-energy, odd-J states are denoted "para." The difference in terminology stems from how the prefixes were determined for each of the spin isomers. The dominant spin isomer at room temperature was denoted "ortho," while the less prevalent form was denoted "para." For hydrogen and tritium, the odd-J states are dominant at room temperature while the even-J states are dominant for deuterium. This leads to orthohydrogen, paradeuterium, and orthotritium corresponding to odd-J states, and parahydrogen, orthodeuterium, and paratritium corresponding to even-J states. The reason for these differences can be explained by quantum mechanics and the degeneracy of the molecules. A detailed discussion of these differences is available in Silvera[6] and Souers.[7]

The ratio of the ortho-para composition of a sample is dependent on temperature, and a singular equilibrium composition will be obtained when a sample is left at a constant temperature for a sufficient length of time. This equilibrated composition is known as "equilibrium deuterium," abbreviated eD_2. When temperatures are sufficiently high (i.e., room temperature), all degenerate molecular configurations are populated. The equilibrated composition at high temperatures is known as "normal deuterium" and is a ratio of the degeneracies of orthodeuterium and paradeuterium. The ratio of molecules in the even-J states, oD_2, to odd-J states, pD_2, is 2:1 for normal deuterium. Normal deuterium has been treated as a pure fluid in this work due to the common need for fluid properties at this ortho-para composition. Unless the spin isomer is specified, the authors are referring to normal deuterium in this work.

3.1. Differences between orthodeuterium and paradeuterium forms

The differences between orthodeuterium and paradeuterium are primarily due to a difference in rotational energy that becomes substantial at low temperatures, where the number of accessible energy levels is limited. Significant deviations in ideal-gas heat capacities exist below 250 K. The maximum difference between oD_2 and pD_2 occurs near 80 K and creates a difference in ideal-gas heat capacities approaching 30%. Figure 1 shows the differences in ideal-gas heat capacities for normal deuterium, orthodeuterium, and paradeuterium. The ideal-gas heat capacities shown in Fig. 1 were calculated using the model described by Le Roy *et al.*[8] Ideal-gas properties derived from heat capacities such as enthalpy and entropy also show significant differences between the ortho and para forms. Therefore, separate ideal-gas equations for nD_2, oD_2, and pD_2 were created to account for differences in ideal-gas properties.

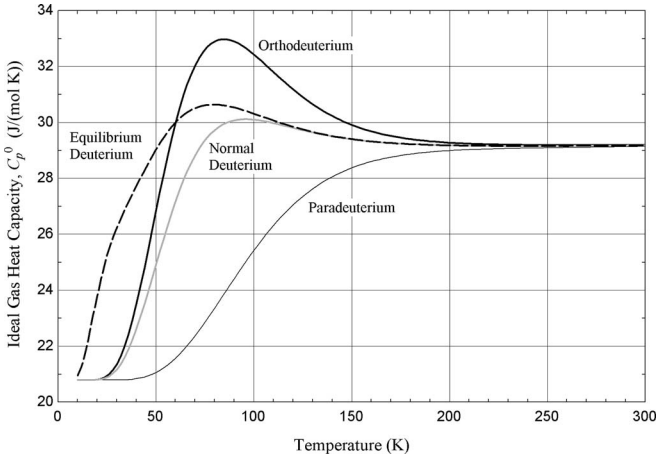

FIG. 1. Calculated ideal-gas heat capacities of normal deuterium, orthodeuterium, and paradeuterium.

Small variations also exist in fluid properties beyond the ideal-gas level. In Knaap and Beenakker's[9] work from 1961, they predicted differences in molar volumes, second virial coefficients, and vapor pressures between orthodeuterium and paradeuterium, based on discrepancies in the dispersion energy that exist due to differences in the polarizability of the nuclear spin isomers. They predicted differences between oD_2 and pD_2 to be less than 0.2% for molar volumes and less than 1% for second virial coefficients at 20 K. These differences will be largest at the triple-point temperature. These deviations are smaller than the uncertainty of the new equation of state. However, Knaap and Beenakker predict deviations of 2.5% between vapor pressures of oD_2 and pD_2 at 20 K. This deviation can be seen in the experimental vapor pressure measurements and is discussed in Sec. 5.2. Although differences in thermophysical properties exist between oD_2 and pD_2, these differences were insufficient to warrant entirely separate real-fluid equations for the different isomers, due to the limited amount of experimental measurements available. The real-fluid equation was developed with normal deuterium measurements. Experimentalists using this equation of state to calculate vapor pressures on any ortho-para composition other than normal deuterium should be aware of these differences, especially near the triple point, since these uncertainties may be larger than the uncertainties reported in this work.

There also exist minor differences in critical-point and triple-point properties between nD_2, oD_2, and pD_2 that have not been considered in this work. In their 1987 review of the triple point of deuterium, Pavese and McConville[10] measured the triple-point temperature of nD_2 and eD_2 to be 18.7240 and 18.6896 K, respectively. There are no critical-point or triple-point properties available in the literature for paradeuterium. Pavese and McConville's triple-point temperature of normal deuterium was used as the triple-point temperature for all of the new deuterium formulations. This is due to the lack of experimental data resulting in a single real-fluid function that is shared by all the deuterium formulations. Thus, all formulations share the same triple-point properties. This will be discussed in greater detail in Sec. 4. The reported temperatures of Pavese and McConville and all other temperatures reported in this work have been updated to the International Temperature Scale of 1990 (ITS-90). The molar mass of deuterium used in this work was 4.0282 g/mol.[11]

4. Equation of State and Ancillary Functions

The new functional form for the oD_2, nD_2, and pD_2 EOS was determined through nonlinear regression of experimental data and fitted constraints. This work presents only information pertaining to the new deuterium formulations. A detailed discussion of modern thermodynamic property formulations has been done by Span.[12]

Modern equations of state are explicit in the molar Helmholtz free energy, a. The Helmholtz free energy is expressed in terms of density and temperature as

$$\frac{a(T,\rho)}{RT} = \alpha(\tau,\delta), \tag{1}$$

where α is the reduced Helmholtz free energy and τ and δ are the reciprocal reduced temperature and reduced density, respectively,

$$\tau = \frac{T_c}{T}, \tag{2}$$

$$\delta = \frac{\rho}{\rho_c}. \tag{3}$$

The subscript c denotes the critical-point property. The reduced Helmholtz free energy contains an ideal-gas contribution, α^0, and a residual real-fluid contribution, α^r. The reduced Helmholtz free energy is expressed as

$$\alpha(\tau,\delta) = \alpha^0(\tau,\delta) + \alpha^r(\tau,\delta). \tag{4}$$

The ideal-gas contribution was fitted based on nonlinear regression of ideal-gas heat capacity data from the literature and will be discussed below. The residual contribution is determined by nonlinear regression of experimental measurements of thermodynamic properties as well as constraints forcing correct fluid behavior in regions with limited or no data. A discussion of the constraints used in the development of the new EOS can be found in Sec. 4.3. The reduced Helmholtz free energy can be used to determine other thermodynamic properties at any state within the designated temperature and pressure limits. The equations used to convert from Helmholtz free energy to other energies, enthalpies, entropies, heat capacities, speed of sound, etc., are given by Span.[12] The regression process used to determine the deuterium EOS was the same as in the hydrogen correlation.[5] In short, weights are given to specified data points and constraints according to their significance and accuracy. Differences between experimentally measured data points and predicted values from the equation of state are minimized according to the weight associated with each data point or constraint. The resulting coefficients and exponents are reported in Secs. 4.1 and 4.2.

4.1. Ideal-gas contributions to the equation of state

The ideal-gas contributions to the EOS that predict caloric properties show significant differences between the ortho and para forms of deuterium. As a result, separate ideal-gas equations were developed for normal deuterium, orthodeuterium, and paradeuterium. The ideal-gas isobaric heat capacity equation is expressed as

$$\frac{c_p^0}{R} = 2.5 + \sum_{k=1}^{N} u_k \left(\frac{v_k}{T}\right)^2 \frac{\exp(v_k/T)}{[\exp(v_k/T)-1]^2}. \tag{5}$$

The parameters and coefficients of Eq. (5) are reported in Table 1 with $N = 12$ for the nD_2 and oD_2 equations and $N = 11$ for the pD_2 equation. The primary ideal-gas isobaric heat capacity data used to determine these parameters and coefficients were reproduced from Le Roy *et al.*[8] Le Roy *et al.* do not specifically state an uncertainty but report that the data are accurate to 0.1 mJ/(K mol), which gives an uncertainty of less than 0.001%. The uncertainty of Eq. (5) is 0.04% with a coverage factor of 2 for all isomers of deuterium presented in this work. It is important to note that Le Roy *et al.* did not account for the differing ortho-para terminology that exists between hydrogen and deuterium. Thus the values reported by Le Roy *et al.* for paradeuterium are actually those of orthodeuterium, and vice versa. This has been corrected in this work. The percent deviation between values calculated from Eq. (5) and values reported in the literature are shown in Fig. 2 for normal deuterium, Fig. 3 for orthodeuterium, and Fig. 4 for paradeuterium.

The ideal-gas Helmholtz free energy portion of the equation of state can be reduced to a dimensionless form given by

$$\alpha^0 = a_1 + a_2\tau + \ln\delta + 1.5\ln\tau + \sum_{k=1}^{N} u_k \ln[1 - \exp(-v_k\tau/T_c)], \tag{6}$$

where the subscript k is the index of terms. The parameters a_1 and a_2 for the new nD_2, oD_2, and pD_2 formulations are reported in Table 2.

TABLE 1. Parameters and coefficients of the normal deuterium, orthodeuterium, and paradeuterium ideal-gas heat capacity equation, Eq. (5)

	Normal deuterium		Orthodeuterium		Paradeuterium	
k	u_k	v_k	u_k	v_k	u_k	v_k
1	−3.54145	7174.1	4.04482	1591	1.28527	5068
2	3.03260	8635	−4.65391	481.6	1.11376	1000.8
3	−3.52422	902.7	−4.65342	472.4	−2.49100	261.5
4	−1.73421	181.1	3.46313	362.2	6.38763	437.2
5	−3.57135	438.5	−4.58637	2038	6.17406	312.3
6	2.14858	5034.2	−4.65030	463.2	−3.13698	382.8
7	6.23107	269.9	−4.65124	491.3	−3.14254	356.8
8	−3.30425	229.9	2.67024	2713.4	−2.29511	294.7
9	6.23098	666.4	15.20455	618.6	−3.37000	682.4
10	−3.57137	452.8	0.87164	8642	1.13634	246
11	3.32901	192	−4.76080	961.7	0.72512	277.1
12	0.97782	1187.6	4.32447	253.2	–	–

4.2. Real-fluid contributions to the equation of state

As discussed in Sec. 3.1, the differences in real-fluid thermodynamic properties that exist between orthodeuterium and paradeuterium are significant in the vapor-pressure measurements. Due to a lack of experimental data for pure oD_2 and pD_2, these differences have not been accounted for in this work. As a result, the real-fluid equations for nD_2, oD_2, and pD_2 are identical for all of the deuterium formulations.

The functional form of the real-fluid contribution to the reduced Helmholtz free energy is

$$\alpha^{\mathrm{r}}(\tau,\delta) = \sum_{i=1}^{8} N_i \delta^{d_i} \tau^{t_i} + \sum_{i=9}^{14} N_i \delta^{d_i} \tau^{t_i} \exp(-\delta^{p_i}) + \sum_{i=15}^{21} N_i \delta^{d_i} \tau^{t_i} \exp[\varphi_i (\delta - D_i)^2 + \beta_i (\tau - \gamma_i)^2]. \quad (7)$$

The first summation is a simple polynomial with exponents on the reduced density and temperature. The second summation contains exponential reduced-density terms that help calculate properties in the liquid and critical regions. The third summation consists of modified Gaussian bell-shaped terms to aid in modeling the critical region where it is very difficult to obtain accurate experimental measurements.

The coefficients and exponents of the equations depend on the constraints and experimental data included in the fitting process. Table 3 lists the experimental data sets[13–48] available for deuterium and distinguishes which data sets were used in the fitting process. Though the second virial coefficients reported by Garberoglio *et al.*[48] were treated as experimental measurements for the purpose of fitting, these values were actually calculated from theory. The first column of Table 3 gives the data referenced, the second column contains the year the data was published; columns 3–6 contain the number of

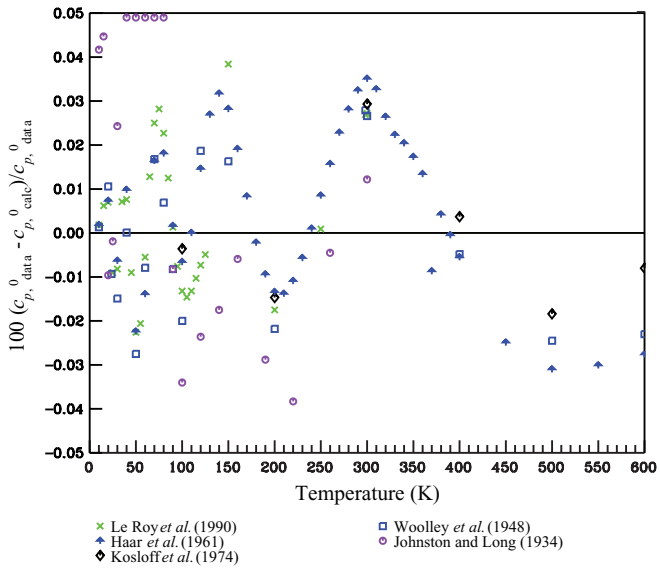

FIG. 2. Comparisons of ideal-gas isobaric heat capacities for normal deuterium to data in the literature.

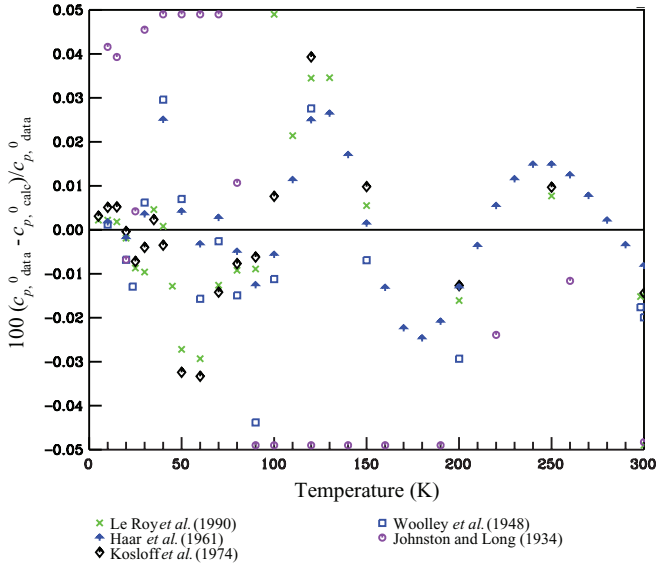

FIG. 3. Comparisons of ideal-gas isobaric heat capacities for orthodeuterium to data in the literature.

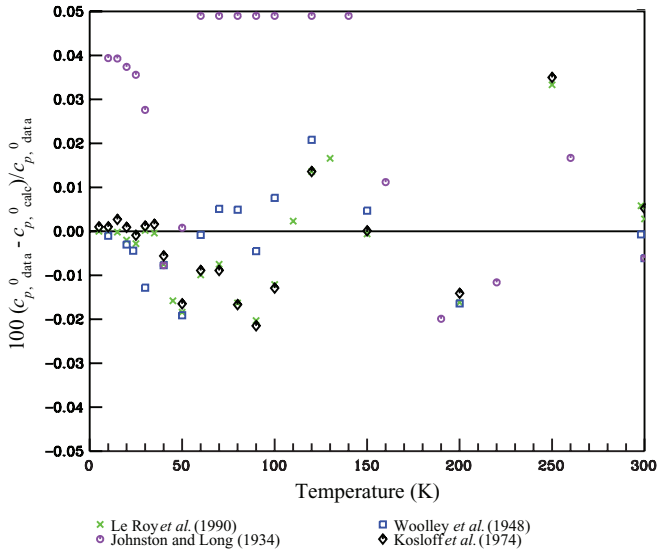

FIG. 4. Comparisons of ideal-gas isobaric heat capacities for paradeuterium to data in the literature.

data points used in the fitting process, the total number of data points, and the temperature and pressure ranges; and the last two columns give the Absolute Average Deviation (AAD) that will be discussed in Sec. 5. The constraints applied in the fitting process will be discussed in Sec. 4.3.

There are bounds on some of the variables to ensure physically correct fluid behavior. Values of d_i, p_i, t_i, γ_i, and D_i are positive, with d_i and p_i as integers. Values of φ_i and β_i are less than zero. The parameters and coefficients of the polynomial and Gaussian terms for the new deuterium EOS are given in Table 4.

4.3. Applied fitting constraints

Due to the limited amount of experimental data available for deuterium, a number of constraints were used to regress the EOS. Constraints are used to force the EOS to demonstrate proper fluid behavior and thermodynamic consistency. Constraints were also used to ensure that the equation demonstrates proper extrapolation behavior at extreme pressures and densities as well as at temperatures approaching absolute zero. A list of the constraints used in the development of the new deuterium EOS is given in Table 5. The first column gives the property or locus to which the constraint is applied. The second column gives the constraint that was used. The "slope" constraint refers to the slope of the constant-property line (isotherm, isobar, etc.) plotted against the respective property over the specified range. The third column gives the range over which the constraint was applied. For example, the first constraint in Table 5 states that the values of the third virial coefficients are positive between 30 and 60 K. The term "all derivatives" refers to the first, second, third, and fourth derivatives. When the constraint is a derivative, the first column represents the property that is being differentiated and the third column gives the property which the derivative is taken with respect to and what is being held constant. As an example, the first constraint involving the isochoric heat capacity c_v states that all derivatives (i.e., first through fourth) of c_v with respect to temperature are positive for a pressure of 4 MPa from 9 to 37 K. The constraints used in this work are "soft" constraints, meaning that the EOS is not required to fully obey the constraint. If a constraint is not obeyed it will add to the overall disagreement between the EOS and the applied constraints and experimental data being fit.

TABLE 2. Coefficients a_1 and a_2 of the normal deuterium, orthodeuterium, and paradeuterium ideal-gas Helmholtz free energy equation, Eq. (6)

	Normal deuterium	Orthodeuterium	Paradeuterium
a_1	−2.0677351753	−2.0672670563	−2.0683998716
a_2	2.4237151502	2.4234599781	2.4241000701

4.4. Fixed state points and ancillary equations

The critical-point and triple-point properties have been treated as fixed state points in this work. These properties are dependent on the ortho-para composition of the fluid. Since the critical-point and triple-point properties are used in the development of the real-fluid component of the EOS and the real-fluid component is identical for the oD_2, nD_2, and pD_2 equations, the critical-point and triple-point properties are the same for all the deuterium formulations. The fixed state points of the new deuterium EOS differ slightly from those used in the McCarty model.[3]

This work used the critical temperature measured by Friedman *et al.*[13] The critical pressure and density were then calculated from the EOS. The most recent triple-point temperature measurement of normal deuterium by Pavese and McConville[10] was selected as the lower-temperature limit for all of the deuterium formulations. The critical-point and triple-point properties for the new deuterium formulations, denoted by this work, and the McCarty EOS are given in Table 6. Note that small differences in critical-point and triple-point properties exist between nD_2, oD_2, and pD_2 that have not been accounted for in this work.

Values along the saturation lines were calculated from the equation of state with the Maxwell criteria (equal Gibbs energies for the liquid and vapor saturation states), and then used to develop ancillary equations. These ancillaries can be useful as initial guesses in the determination of the saturation states from the equation of state, but the calculated values should not be reported as the true saturation state. Publications such as those by Span[12] should be reviewed to determine the best procedure for calculating saturation properties. Vapor pressures are represented with the equation

$$\ln\left(\frac{p_\sigma}{p_c}\right) = \frac{T_c}{T}\left[N_1\theta + N_2\theta^{1.5} + N_3\theta^{2.83} + N_4\theta^{4.06} + N_5\theta^{5.4}\right], \tag{8}$$

where $N_1 = -5.5706$, $N_2 = 1.7631$, $N_3 = -0.5458$, $N_4 = 1.2154$, $N_5 = -1.1556$, $\theta = (1 - T/T_c)$, and p_σ is the vapor pressure. The saturated liquid density can be represented by

TABLE 3. Experimental data sets and AAD from the new deuterium equation of state and McCarty equation of state

Author	Year	Total points fit	Total points	Temperature range (K)	Pressure range (MPa)	AAD from new EOS	AAD from McCarty
			p-ρ-T				
Friedman *et al.*[13]	1954	11	44	20.3–38.1	8.6–11.02	0.227	0.193
Clusius and Bartholome[14]	1935	–	8	18.8–20.5	Sat	0.295	0.433
Hoge and Lassiter[15]	1951	–	50	37.2–41.2	1.42–2.23	7.886	14.303
Kerr[16]	1952	–	5	19.5–24.2	Sat	0.267	0.297
Liebenberg *et al.*[17]	1977	6	1340	75–300	200–2000	3.708	35.020
Michels and Goudeket[18]	1941	–	277	273.2–423.2	0.9–305.1	0.499	0.506
Michels *et al.*[19]	1959	67	417	98.2–423.2	0.6–283.8	0.156	0.174
Rudenko and Slyusar[20]	1969	–	19	18.7–34.9	Sat	1.222	0.824
Rudenko and Slyusar[21]	1968	–	24	20.4–34.8	Sat	1.429	0.873
Cramer[22]	1965	–	10	298.1	10.2–141.9	0.093	0.110
David and Hamann[23]	1953	–	16	64.5–78.9	15.2–91.2	1.001	2.169
Beenakker *et al.*[24]	1959	–	10	20.4	0.015–0.034	0.461	3.067
Bartholome[25]	1936	1	25	19.70–20.97	0.7–9.2	0.231	0.274
Knaap *et al.*[26]	1962	–	9	27.8–71.8	0.032–0.084	2.343	2.705
			Saturation heat capacity				
Kerr *et al.*[27]	1951	3	8	19.9–22.7	Sat	1.527	6.308
Brouwer *et al.*[28]	1970	2	18	24–27.4	Sat	1.420	15.998
Grenier and White[29]	1964	–	3	20–22	Sat	1.596	5.214
Clusius and Bartholome[14]	1935	–	8	19.4–21.7	Sat	9.832	10.490
			Vapor pressure				
Brickwedde *et al.*[30]	1935	–	4	18.7–20.4	Sat	2.786	15.939
Friedman *et al.*[31]	1951	3	18	29–38.1	Sat	0.909	4.799
Grilly[32]	1951	–	29	18.9–27.8	Sat	0.208	10.951
Kerr *et al.*[27]	1951	–	7	18.6–23.7	Sat	2.829	8.536
Lewis and Hanson[33]	1934	–	5	18.7–20.3	Sat	5.039	13.017
Scott *et al.*[34]	1934	2	6	15.2–20.3	Sat	0.577	13.719
Hoge and Arnold[35]	1951	1	79	18.8–38.2	Sat	0.984	9.600
Hiza[36]	1972	7	14	20–34	Sat	0.375	8.989
Meckstroth and White[37,a]	1971	–	87	17.2–22.5	Sat		
			Speed of sound				
Bezuglyi and Minyafaev[38]	1968	–	2	19–20	Sat	5.049	1.994
Brody *et al.*[39]	1981	–	11	298	500–5500	15.635	51.065
Gusewell *et al.*[40]	1970	3	7	25–31	Sat	0.135	5.615
Liebenberg *et al.*[17]	1977	3	1340	75–300	200–2000	6.631	37.765
van Itterbeek and Thys[41]	1938	–	3	239–297	0.08–0.09	0.239	0.245
van Itterbeek and Vandoninck[42]	1943	–	46	19–21	0.006–0.035	0.127	1.891
van Itterbeek and van Paemel[43]	1938	–	2	20.36	0.013–0.03	0.513	1.994
van Itterbeek and Vermaelen[44]	1942	–	28	68–290.6	0.04–0.1	1.507	1.404
			Second virial coefficient				
Michels and Goudeket[18]	1941	–	21	273.2–423.2	–	0.870	13.992
Michels *et al.*[45]	1960	–	17	98.2–423.2	–	0.263	9.732
Beenakker *et al.*[24]	1959		1	20.4	–	7.154	181.000
Knaap *et al.*[26]	1962	–	2	20.51–21.55	–	6.324	172.150
Varekamp and Beenakker[46]	1959	–	5	18–21	–	7.938	193.200
Schafer[47]	1937	–	22	23.2–273.2	–	1.478	49.585
Garberoglio *et al.*[48]	2012	11	33	15–2000	–	0.135	21.554

[a]These data were not included in the comparison due to reported vapor-pressure differences between eD2 and pD2 compositions.

the ancillary equation

$$\frac{\rho'}{\rho_c} = 1 + N_1\theta^{0.512} + N_2\theta^{1.12} + N_3\theta^{1.8} + N_4\theta^{2.55} + N_5\theta^{3.4} + N_6\theta^{4.4}, \quad (9)$$

where $N_1 = 3.3769$, $N_2 = -5.3693$, $N_3 = 11.943$, $N_4 = -17.361$, $N_5 = 15.170$, $N_6 = -6.3079$, $\theta = (1 - T/T_c)$, and ρ' is the saturated liquid density. The saturated vapor density can be represented by the equation

$$\ln\left(\frac{\rho''}{\rho_c}\right) = N_1\theta^{0.528} + N_2\theta^{2.03} + N_3\theta^{3.6} + N_4\theta^{5} + N_5\theta^{6.5} + N_6\theta^{9}, \quad (10)$$

where $N_1 = -3.8111$, $N_2 = -7.3624$, $N_3 = 2.2294$, $N_4 = -21.443$, $N_5 = 12.796$, $N_6 = -31.334$, $\theta = (1 - T/T_c)$, and ρ'' is the saturated vapor density.

TABLE 4. Parameters and coefficients of the new deuterium equation of state, Eq. (7)

i	N_i	t_i	d_i	p_i	φ_i	βi	γ_i	D_i
1	0.006267958	1	4	–				
2	10.53609	0.462	1	–				
3	−10.14149	0.5584	1	–				
4	0.356061	0.627	2	–				
5	0.1824472	1.201	3	–				
6	−1.129638	0.309	1	–				
7	−0.0549812	1.314	3	–				
8	−0.6791329	1.1166	2	–				
9	1.347918	1.25	2	1				
10	−0.8657582	1.25	2	1				
11	1.719146	1.395	1	2				
12	−1.917977	1.627	1	2				
13	0.1233365	1	3	2				
14	−0.07936891	2.5	2	2				
15	1.686617	0.635	1	–	−0.868	−0.613	0.6306	1.46
16	−4.240326	0.664	1	–	−0.636	−0.584	0.711	1.7864
17	1.857114	0.7082	2	–	−0.668	−0.57	0.6446	1.647
18	−0.5903705	2.25	3	–	−0.65	−1.056	0.8226	0.541
19	1.520171	1.524	3	–	−0.745	−1.01	0.992	0.969
20	2.361373	0.67	1	–	−0.782	−1.025	1.2184	1.892
21	−2.297315	0.709	3	–	−0.693	−1.029	1.203	1.076

TABLE 5. Constraints applied to the fitting process for the deuterium equation of state

Property/ locus	Constraint[a]	Range
Third virial coefficient	Positive values	$T = 30 \rightarrow 60$ K
Third virial coefficient	All derivatives change from negative to positive	$\lg(\rho) = -5 \rightarrow 1.4$
Phase identification parameter	All derivatives change from negative to positive	Liquid saturation line, $\rho = 20 \rightarrow 45$ mol/dm^3
Rectilinear diameter	Zero curvature	Saturated Liquid, $T = 0.8T_c \rightarrow T_c$
Pressure	Negative slope	$T = 1$ K, $\rho = 43 \rightarrow 49$ mol/dm^3
Pressure	Positive curvature	$T = 0.977T_c$, $\rho = 1.2\rho_c \rightarrow 1.5\rho_c$
Pressure	Zero slope	$T = T_c$, $\rho = 0.975\rho_c \rightarrow 0.985\rho_c$
Pressure	Zero slope	$T = T_c$, $\rho = 1.015\rho_c \rightarrow 1.025\rho_c$
$dp/d\rho$	Values are positive	$T = T_c$, $\rho = 0.97\rho_c \rightarrow 0.999\rho_c$
$dp/d\rho$	Values are positive	$T = T_c$, $\rho = 1.001\rho_c \rightarrow 1.03\rho_c$
$d^2p/d\rho^2$	Values are negative	$T = T_c$, $\rho = 0.97\rho_c \rightarrow 0.999\rho_c$
$d^2p/d\rho^2$	Values are positive	$T = T_c$, $\rho = 1.001\rho_c \rightarrow 1.03\rho_c$
$d^2p/d\rho^2$	Positive slope	$T = T_c$, $\rho = 1.001\rho_c \rightarrow 1.03\rho_c$
c_v	All derivatives are positive	$p = 4$ MPa, $T = 9 \rightarrow 37$ K
c_v	All derivatives are positive	Liquid saturation line, $T = 9 \rightarrow 37$ K
c_v	All derivatives are positive	Vapor saturation line, $T = 5 \rightarrow 37$ K
c_v	All derivatives are positive	$p = 300$ MPa, $T = 16 \rightarrow 37$ K
c_v	All derivatives are positive	$\rho = 50$ mol/dm^3, $T = 15 \rightarrow 37$ K
ρ	All derivatives are negative	Liquid saturation line, $T = 0.96T_c \rightarrow T_c$
ρ	All derivatives are positive	Vapor saturation line, $T = 0.96T_c \rightarrow T_c$
Speed of sound	All derivatives are negative	Liquid saturation line, $T = 5 \rightarrow 37$ K
Gruneisen	All derivatives are negative	Liquid saturation line, $T = 7 \rightarrow 32$ K
Compressibility	Positive slope	$T = 30$ K, $\rho = 0.1 \rightarrow 2.1$ mol/dm^3

[a]The phrase "all derivatives" refers to the first, second, third, and fourth derivative.

TABLE 6. Critical and triple-point properties for the new deuterium EOS (left) and the McCarty EOS (right)

	Temperature (K)		Pressure (MPa)		Density (mol/L)	
	This work	McCarty[3]	This work	McCarty[3]	This work	McCarty[3]
Critical point	38.34	38.334	1.665	1.6653	17.6	17.327
Triple point	18.724	18.7	0.017257	0.019462	43.283	43.365

5. Comparisons of the New Equation of State to Experimental Data

Deviation plots have been created to compare the accuracy of calculated values with the new normal deuterium EOS to experimental measurements. The comparisons referenced in this section show deviations using the McCarty EOS (Ref. 3) on the bottom or right side of each figure and the new nD_2 EOS on the top or left side of each figure. The experimental data presented in this section contain all experimental data available for deuterium with no distinction between ortho and para compositions.

A primary metric in determining the accuracy of the EOS is given by the AAD for each data set, which is calculated by

$$\mathrm{AAD} = \frac{1}{n}\sum_{i=1}^{n}|\%\Delta X_i|, \tag{11}$$

$$\%\Delta X = 100\left(\frac{X_{\mathrm{data}} - X_{\mathrm{calc}}}{X_{\mathrm{data}}}\right). \tag{12}$$

The density, saturated heat capacity, vapor pressure, speed of sound, and second virial coefficients have been included in the AAD comparisons. The AAD for the McCarty and new EOS have been included in Subsections 5.1 and 5.2. Experimental data[13–48] shown in tables and figures in this work are referenced by the author(s) and year of publication. As discussed in Sec. 4.2, Table 3 lists the experimental data sets available for deuterium. The AAD from the new EOS and McCarty EOS are provided in the last two columns of Table 3.

5.1. Ideal-gas property comparisons

The ideal-gas properties for normal deuterium, orthodeuterium, and paradeuterium are compared in this section. The McCarty EOS considered ideal-gas properties for normal deuterium only when it was developed and thus will have a deviation as large as 10% for orthodeuterium and 30% for paradeuterium. The differences between ideal-gas heat capacities for nD_2, oD_2, and pD_2 can be seen in Fig. 1. The ideal-gas parameters and coefficients for normal deuterium, orthodeuterium, and paradeuterium were regressed to the most accurate prediction of the ideal-gas isobaric heat capacities (Refs. 8 and 49–52). Above 250 K, the ideal-gas heat capacities of oD_2, nD_2, and pD_2 converge as the differences in rotational energies become less significant. Thus, for temperatures above 300 K, deviations have been plotted only for normal deuterium.

In all of the deuterium formulations, the ideal-gas heat capacity data from Le Roy *et al.*[8] have been given priority up to 300 K. The ideal-gas heat capacity data for normal deuterium were not directly calculated by Le Roy *et al.*, but the values of normal deuterium were calculated from the ideal-gas heat capacities of orthodeuterium and paradeuterium as described in Leachman and Richardson.[4] Above 300 K, the data set of Haar *et al.*[50] was given priority.

Comparisons of calculated values from the normal deuterium, orthodeuterium, and paradeuterium ideal-gas equations to tabulated data from the literature are shown in Figs. 2–4, respectively. For oD_2 and pD_2 the estimated uncertainty is 0.04% from 10 to 300 K. The estimated uncertainty in ideal-gas heat capacities for nD_2 is 0.04% from 10 to 600 K.

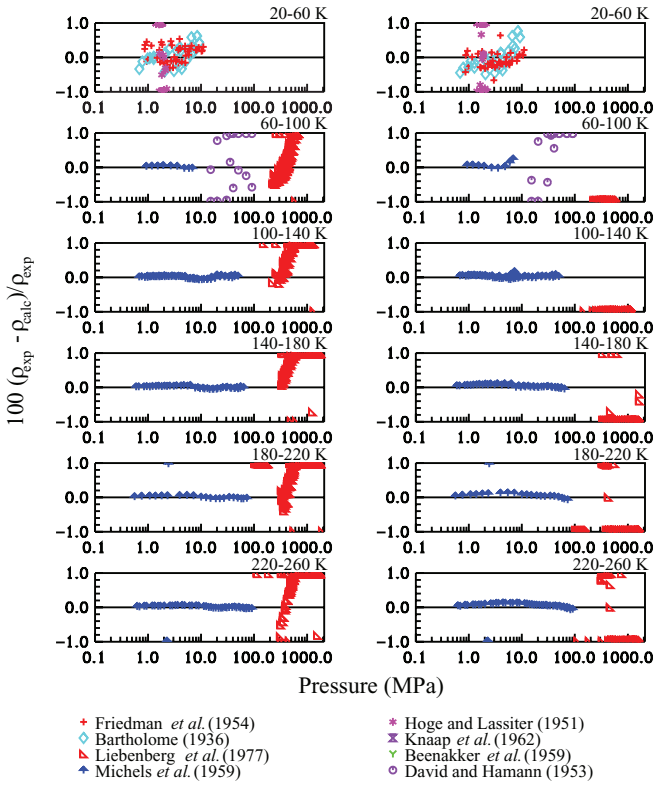

FIG. 5. Comparisons of calculated densities for the new deuterium EOS (left) and the deuterium EOS of McCarty (right) to experimental data from 20 to 260 K.

5.2. Thermophysical property comparisons

The residual contribution to the EOS accounts for real-fluid behavior. Because the real-fluid equations in this work are the same for nD_2, oD_2, and pD_2, the thermophysical properties that depend only on residual contributions (p-ρ-T, virial coefficients, etc.) will be identical. Calculated comparisons have been made for density, vapor pressure, speed of sound, saturated heat capacity, and second virial coefficients and are valid for all of the deuterium formulations within the specified uncertainty, with the exception of vapor pressure, which is discussed below. If the ortho-para composition was not specified by the experimentalist, it was assumed to be normal deuterium.

Figures 5 and 6 display pressure versus density deviations. They are separated into temperature increments indicated in the top right corner of each plot. The deviations for the new EOS are displayed on the left side and the deviations for the McCarty EOS on the right side. At temperatures above 90 K, the data of Michels *et al.*[19] were used as the primary data set. The data of Liebenberg *et al.*[17] were measured at pressures up to 2000 MPa and were used as a secondary data set to ensure accurate high-pressure behavior.

Figure 7 shows the difference in second virial coefficients plotted against temperature. The only second virial coefficient

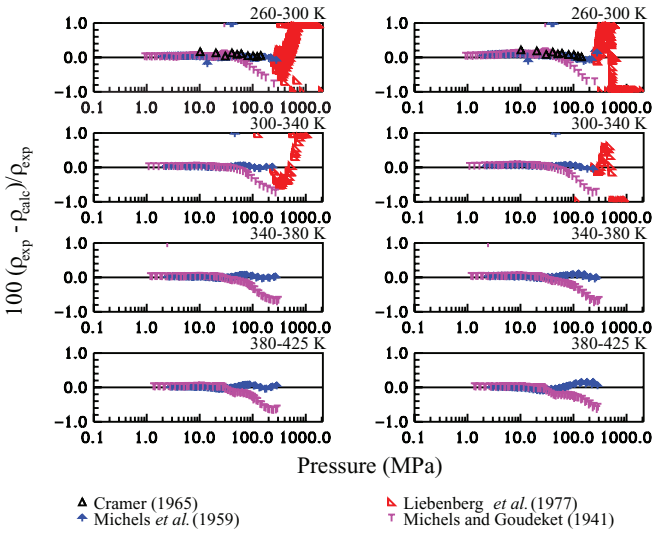

FIG. 6. Comparisons of calculated densities for the new deuterium EOS (left) and the deuterium EOS of McCarty (right) to experimental data from 260 to 425 K.

data used in the regression process were those of Garberoglio *et al.*[48] The data of Garberoglio *et al.* have a maximum expanded uncertainty of 3.76 cm^3/mol at 15 K. These data agree with the new deuterium equation of state within its own uncertainty over the full range of data from 15 to 2000 K. Figure 8 shows an enlarged plot of the difference in second virial coefficients from the new EOS up to 1000 K.

Figure 9 compares the calculated vapor pressures of the new EOS (top) and the McCarty EOS (bottom) to experimental data. In the range from 20 to 34 K, the data by Hiza[36] were chosen as primary. Between the triple point and 20 K, the measurements by Scott *et al.*[34] were chosen as primary. From 34 K to the critical point, the data of Friedman *et al.*[13] were

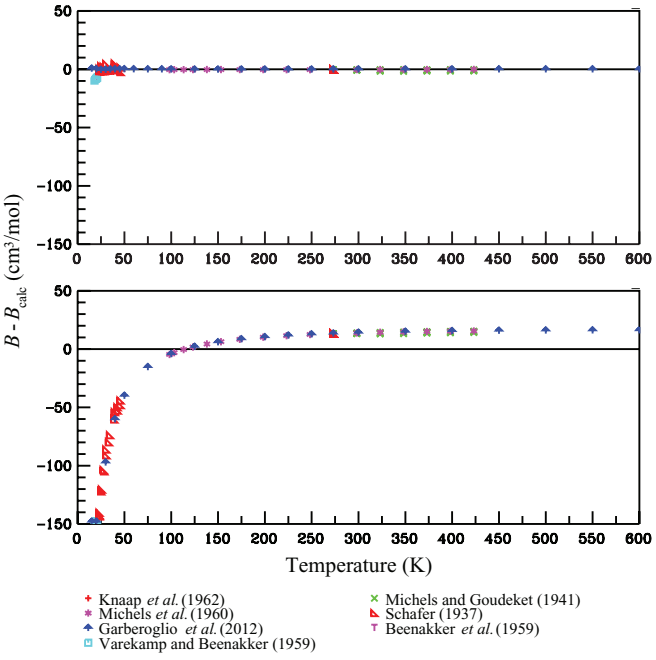

FIG. 7. Comparisons of calculated second virial coefficients to data plotted versus temperature for the new deuterium EOS (top) and the EOS of McCarty (bottom).

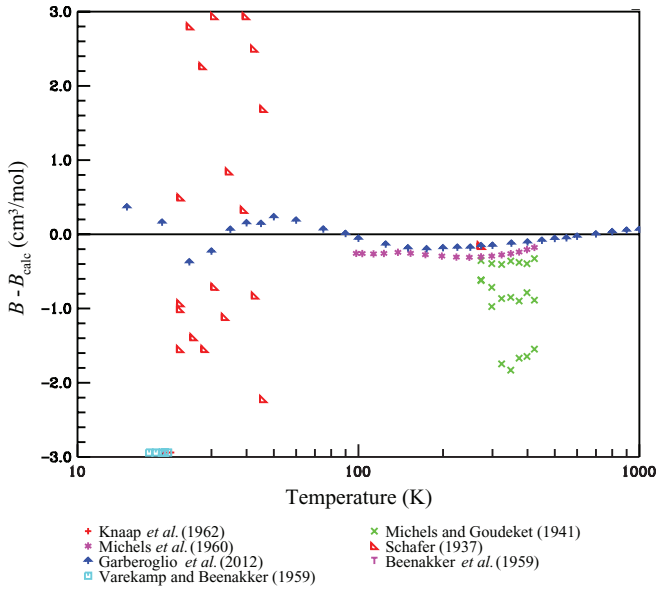

FIG. 8. Comparisons of calculated second virial coefficients to data plotted versus temperature extrapolated to 1000 K for the new deuterium EOS.

chosen as primary. The EOS for deuterium was developed with vapor pressures for normal deuterium. As discussed previously, there are deviations between orthodeuterium and paradeuterium vapor pressures that have not been accounted for in this work. This deviation can be seen in Fig. 9 by examination of the data of Kerr *et al.*[27] at temperatures below 24 K. The vapor pressure measurements of Kerr *et al.*[27] were conducted using 97.8% pure orthodeuterium. At 20 K, their data show a deviation of approximately 3%. Thus, the experimental data are in agreement with the predicted deviations of Knapp and Beenakker[9] discussed in Sec. 3.1.

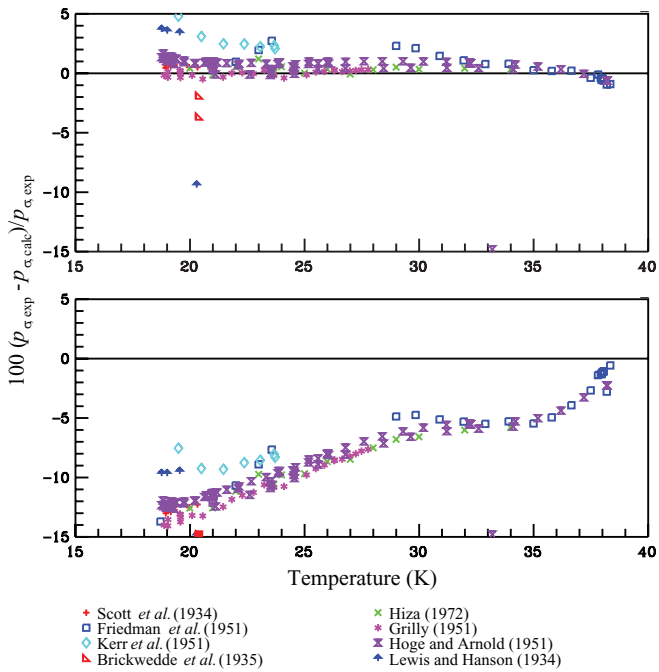

FIG. 9. Comparisons of calculated vapor pressures for the new deuterium EOS (top) and the deuterium EOS of McCarty (bottom) to experimental data.

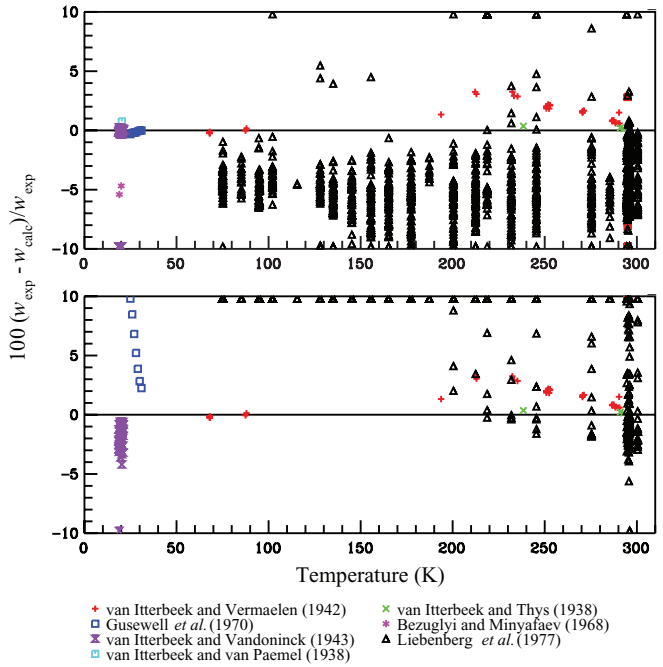

FIG. 10. Comparisons of calculated speeds of sound plotted versus temperature for the new deuterium EOS (top) and the deuterium EOS of McCarty (bottom) to experimental data. Note that the amount of experimental data plotted is the same in both the top and bottom plot. However, experimental data that is outside of the range of the *y* axis appear as a single point though it is actually many points overlapping that have an uncertainty greater than the set bounds.

Figure 10 compares the calculated speed of sound of the new deuterium EOS (top) and that of McCarty (bottom) to experimental data. The data set of Gusewell *et al.*[40] was the primary data set used for saturated liquid between 25 and 31 K. The data set of van Itterbeek and Vandoninck[42] was chosen as primary for temperatures between 19 and 21 K. Only three data points were used from the measurements of Liebenberg *et al.*[17] conducted at high pressures (up to 2 GPa), due to discrepancies in the data and the extreme pressure range of the data.

Deviations in saturation heat capacity are shown in Fig. 11. The most recent data sets of Brouwer *et al.*[28] and Grenier and White[29] were given priority. The data set of Clusius and Bartholome[14] shows significant deviation from the new EOS

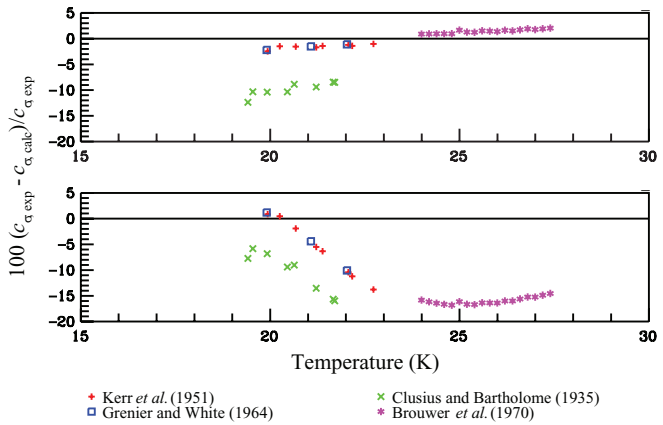

FIG. 11. Comparisons of calculated saturation heat capacities for the new deuterium EOS (top) and the EOS of McCarty (bottom) to experimental data.

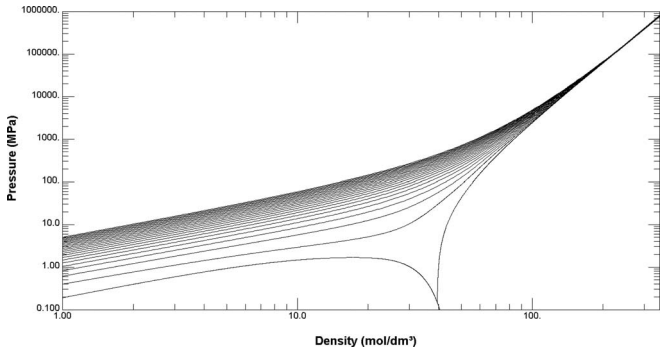

FIG. 12. Pressure versus density diagram for the new normal deuterium EOS. (Isotherms are shown in 25 K increments from 25 to 600 K.)

and the other available data in that temperature range. Considering the year the experiment was conducted and the large deviation from more recent data sets, the Clusius and Bartholome data were neglected in the formulation of the new EOS.

5.3. Function limits and extrapolation behavior

To evaluate the behavior of the equation of state at extreme conditions, it is useful to plot constant-property lines for various thermodynamic relations. It is important to have proper extrapolation behavior well below the triple-point temperature and well above the upper pressure and density limits. If the equation shows proper extrapolation behavior outside the valid range, it is likely that the equation will also behave properly within the valid range. Figure 12 shows the isothermal behavior of the new normal deuterium EOS at extreme pressures and densities. Figure 13 shows a pressure-density diagram with isotherms (from 6 to 54 K) in the two-phase region for the new deuterium equation of state. The isotherms in the pressure-density diagram do not cross the saturation boundary line (shown in bold) within the two-phase region, which would be unphysical, down to 6 K. Though there is no vapor-liquid two-phase region above the critical temperature of 38.34 K or below the triple-point temperature of 18.724 K, Fig. 13 shows that the EOS behaves in a theoretically correct manner well above the critical temperature and well below the triple-point temperature. Thus, the physical two-phase region between the triple point and critical point must also behave correctly.

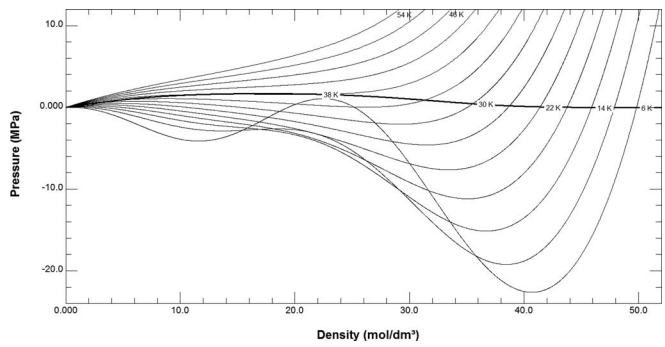

FIG. 13. Pressure versus density diagram showing isotherms (from 6 to 54 K) in the two-phase region for the new deuterium EOS.

6. Results and Recommendations for Future Research

A new equation of state has been developed for deuterium containing separate ideal-gas equations for normal deuterium, orthodeuterium, and paradeuterium. The nD_2, oD_2, and pD_2 formulations predict different ideal-gas properties but have identical real-fluid equations due to the lack of experimental data for orthodeuterium and paradeuterium. The EOS represents the experimental data used in its development to within the estimated uncertainty of the data and generally represents all experimental data to within their estimated uncertainties. The formulations extend the range of reliable property predictions to 2000 MPa and 600 K. The upper pressure limit corresponds to the maximum pressure limits of the data of Liebenberg *et al.*[17] The upper temperature limit of 600 K was determined by examining the uncertainty of the experimental data and the extrapolation behavior of the EOS. Though experimental data only exist up to 423 K, the formulations agree with second virial coefficients from theory up to 2000 K and extrapolate to extreme temperatures without obvious deviations.

Independent ideal-gas equations have been developed for nD_2, oD_2, and pD_2 to obtain correct ideal-gas behavior for the various forms of deuterium. Ideal-gas heat capacity predictions for nD_2, oD_2, and pD_2 have an estimated uncertainty of 0.04%. The estimated combined uncertainty with a coverage factor of 2 for primary data sets in the new deuterium EOS for densities (shown in Figs. 5 and 6) are 1% for temperatures from the triple-point temperature to 90 K, 0.1% from 90 to 425 K, and 1% from 425 to 600 K for pressures below 300 MPa. For pressures ranging from 300 to 1000 MPa the estimated uncertainty is 2.5%, and for pressures approaching 2000 MPa the uncertainty rises to 4%. Uncertainties in saturated liquid densities are 3%. Second virial coefficients have a difference of less than 0.5 cm^3/mol over the entire temperature range of the EOS, as shown in Fig. 8. Uncertainties in vapor pressures are shown in Fig. 9 and are 2% for normal deuterium but deviations of up to 5% may exist for pure orthodeuterium and paradeuterium at temperatures approaching the triple point. Speed-of-sound predictions are accurate within 1% in the liquid region but rise to 5% at moderate temperatures and pressures approaching 2000 MPa.

Acknowledgments

A preliminary account of this work was presented at the 18th Symposium on Thermophysical Properties in Boulder, CO, June 2012. We thank Dr. A. Harvey from NIST for his very helpful suggestions and new work on the virial coefficients of hydrogen isotopes. We thank Stefan Herrig for fitting the ancillary equations.

7. Appendix

Table 7 provides calculated thermodynamic properties at saturation for deuterium. The functions used to calculate thermodynamic properties from Eq. (4) can be found in Span[12] and Lemmon and McLinden.[53]

TABLE 7. Tabulated thermodynamic properties of normal deuterium at saturation

T (K)	p (kPa)	Liquid ρ (kg/m^3)	Vapor ρ (kg/m^3)	Liquid h (kJ/kg)	Vapor h (kJ/kg)	Liquid s (kJ/kg K)	Vapor s (kJ/kg K)	Liquid C_v (kJ/kg K)	Vapor C_v (kJ/kg K)	Liquid C_p (kJ/kg K)	Vapor C_p (kJ/kg K)	Liquid w (m/s)	Vapor w (m/s)
18.724	17.189	174.630	0.455	−30.450	286.160	−1.415	15.494	3.355	3.143	5.627	5.364	1085.50	250.95
19	19.422	173.990	0.508	−28.881	287.350	−1.333	15.311	3.358	3.148	5.674	5.383	1079.80	252.53
20	29.425	171.660	0.737	−23.077	291.490	−1.038	14.690	3.371	3.167	5.852	5.464	1058.60	257.98
21	42.932	169.270	1.035	−17.074	295.380	−0.749	14.130	3.383	3.190	6.044	5.563	1036.60	262.99
22	60.638	166.800	1.412	−10.856	298.980	−0.465	13.619	3.396	3.216	6.252	5.683	1013.60	267.56
23	83.277	164.250	1.880	−4.404	302.260	−0.184	13.149	3.410	3.247	6.477	5.826	989.48	271.68
23.661	101.325	162.510	2.246	−0.002	304.240	0.000	12.858	3.420	3.269	6.638	5.935	972.85	274.17
24	111.60	161.610	2.453	2.301	305.200	0.094	12.715	3.425	3.281	6.724	5.996	964.09	275.37
25	146.40	158.870	3.144	9.282	307.750	0.370	12.309	3.442	3.318	6.996	6.197	937.27	278.61
26	188.45	156.020	3.970	16.565	309.880	0.645	11.927	3.461	3.360	7.298	6.436	908.93	281.40
27	238.58	153.040	4.949	24.181	311.560	0.920	11.564	3.484	3.405	7.640	6.722	878.92	283.75
28	297.60	149.920	6.104	32.168	312.710	1.197	11.216	3.510	3.455	8.031	7.067	847.14	285.66
29	366.37	146.640	7.461	40.571	313.300	1.475	10.879	3.541	3.509	8.489	7.488	813.47	287.11
30	445.75	143.160	9.055	49.449	313.220	1.757	10.550	3.576	3.568	9.036	8.013	777.76	288.11
31	536.67	139.440	10.931	58.879	312.400	2.046	10.223	3.616	3.632	9.712	8.681	739.87	288.66
32	640.08	135.420	13.150	68.966	310.670	2.342	9.895	3.663	3.702	10.576	9.562	699.60	288.75
33	757.06	131.030	15.802	79.861	307.840	2.650	9.558	3.715	3.778	11.741	10.775	656.70	288.42
34	888.79	126.130	19.025	91.800	303.590	2.976	9.205	3.776	3.862	13.421	12.555	610.82	287.72
35	1036.7	120.480	23.053	105.180	297.410	3.329	8.821	3.846	3.954	16.103	15.430	561.44	286.83
36	1202.6	113.640	28.340	120.760	288.290	3.727	8.381	3.929	4.057	21.143	20.869	507.68	286.20
37	1389.2	104.540	35.985	140.400	273.910	4.219	7.827	4.032	4.173	34.179	34.920	447.68	287.25
38	1600.6	88.550	50.659	172.270	244.900	5.009	6.920	4.187	4.300	132.060	137.920	374.12	297.24
38.34	1679.6	69.406	69.406	208.480	208.480	5.931	5.931	4.306[a]	4.306[a]	–	–	–	–

[a]Since the EOS is an analytical Helmholtz function it gives a finite value at the critical temperature. However, the theory of critical phenomena of real fluids states there is a weak divergence of C_v at the critical point.

8. References

[1]I. A. Richardson and J. W. Leachman, AIP Conf. Proc. **1434**, 1841 (2012).
[2]E. W. Lemmon, M. L. Huber, and M. O. McLinden, Standard Reference Data Program #23, REFPROP Version 9.0 (National Institute of Standards and Technology, Gaithersburg, Maryland, 2010).
[3]R. D. McCarty, *Correlations for the Thermophysical Properties of Deuterium* (National Institute of Standards and Technology, Boulder, CO, 1989), unpublished.
[4]J. W. Leachman and I. A. Richardson, *Proceedings of the International Institute of Refrigeration, Twelfth Cryogenics 2012 Conference*, Dresden, Germany, 11–14 September 2012.
[5]J. W. Leachman, R. T. Jacobsen, S. G. Penoncello, and E. W. Lemmon, J. Phys. Chem. Ref. Data **38**, 721 (2009).
[6]I. F. Silvera, Rev. Mod. Phys. **52**, 393 (1980).
[7]P. C. Souers, *Hydrogen Properties for Fusion Energy* (University of California Press, Los Angeles, 1986).
[8]R. J. Le Roy, S. G. Chapman, and F. R. W. McCourt, J. Phys. Chem. **94**, 923 (1990).
[9]H. F. P. Knaap and J. J. M. Beenakker, Physica **27**, 523 (1961).
[10]F. Pavese and G. T. McConville, Metrologia **24**, 107 (1987).
[11]G. Audi, A. H. Wapstra, and C. Thibault, Nucl. Phys. A **729**, 337 (2003).
[12]R. Span, *Multiparameter Equations of State: An Accurate Source of Thermodynamic Property Data* (Springer, New York, 2000).
[13]A. S. Friedman, M. Trzeciak, and H. L. Johnston, J. Am. Chem. Soc. **76**, 1552 (1954).
[14]K. Clusius and E. Bartholome, Z. Phys. Chem. **30B**, 237 (1935).
[15]H. J. Hoge and J. W. Lassiter, J. Res. Natl. Bur. Stand. **47**, 75 (1951).
[16]E. C. Kerr, J. Am. Chem. Soc. **74**, 824 (1952).
[17]D. H. Liebenberg, R. L. Mills, and J. C. Bronson, Los Alamos Report No. 7018-MS, 1977.
[18]A. Michels and M. Goudeket, Physica **8**, 353 (1941).
[19]A. Michels, W. De Graaff, T. Wassenaar, J. M. H. Levelt, and P. Louwerse, Physica **25**, 25 (1959).
[20]N. S. Rudenko and V. P. Slyusar, Zh. Fiz. Khim. **43**, 781 (1969).
[21]N. S. Rudenko and V. P. Slyusar, Zh. Fiz. Khim. **42**, 242 (1968).
[22]J. D. Cramer, Los Alamos Report No. 3250-MS, 1965.
[23]H. G. David and S. D. Hamann, Trans. Faraday Soc. **49**, 711 (1953).
[24]J. J. M. Beenakker, F. H. Varekamp, and A. van Itterbeek, Physica **25**, 9 (1959).
[25]E. Bartholome, Z. Phys. Chem. **33B**, 387 (1936).
[26]H. F. P. Knaap, M. Knoester, C. M. Knobler, and J. J. M. Beenakker, Physica **28**, 21 (1962).
[27]E. C. Kerr, E. B. Rifkin, H. L. Johnston, and J. T. Clarke, J. Am. Chem. Soc. **73**, 282 (1951).
[28]J. P. Brouwer, A. M. Vossepoel, C. J. N. Vam Den Meijdenberg, and J. J. M. Beenakker, Physica **50**, 125 (1970).
[29]G. Grenier and D. White, J. Chem. Phys. **40**, 3015 (1964).
[30]F. G. Brickwedde, R. B. Scott, and H. S. Taylor, J. Chem. Phys. **3**, 653 (1935).
[31]A. S. Friedman, D. White, and H. L. Johnston, J. Am. Chem. Soc. **73**, 1310 (1951).
[32]E. R. Grilly, J. Am. Chem. Soc. **73**, 843 (1951).
[33]G. N. Lewis and W. T. Hanson Jr., J. Am. Chem. Soc. **56**, 1687 (1934).
[34]R. B. Scott, F. G. Brickwedde, H. C. Urey, and M. H. Wahl, J. Chem. Phys. **2**, 454 (1934).
[35]H. J. Hoge and R. D. Arnold, J. Res. Natl. Bur. Stand. **47**, 63 (1951).
[36]M. J. Hiza, *Liquid-Vapor Equilibrium in the Binary Systems of He^4 and He^3 with nD_2 and nH_2*, NBS Technical Note 621 (U.S. Government Printing Office, Washington, 1972).
[37]W. K. Meckstroth and D. White, J. Chem. Phys. **54**, 3723 (1971).
[38]P. A. Bezuglyi and R. Kh. Minyafaev, Sov. Phys. Solid State **9**, 2854 (1968).
[39]E. M. Brody, H. Shimizu, H. K. Mao, P. M. Bell, and Wm. A. Bassett, J. Appl. Phys. **52**, 3583 (1981).
[40]D. Gusewell, F. Schmeissner, and J. Schmid, Cryogenics **10**, 150 (1970).
[41]A. van Itterbeek and L. Thys, Physica **5**, 889 (1938).
[42]A. van Itterbeek and W. Vandoninck, Physica **10**, 481 (1943).
[43]A. van Itterbeek and O. van Paemel, Physica **5**, 845 (1938).
[44]A. van Itterbeek and R. Vermaelen, Physica **9**, 345 (1942).
[45]A. Michels, W. De Graaff, and C. A. Ten Seldam, Physica **26**, 393 (1960).
[46]F. H. Varekamp and J. J. M. Beenakker, Physica **25**, 889 (1959).
[47]K. Schafer, Z. Phys. Chem. **36**, 85 (1937).
[48]G. Garberoglio, P. Jankowski, K. Szalewicz, and A. H. Harvey, J. Chem. Phys. **137**, 154308 (2012).
[49]H. W. Woolley, R. B. Scott, and F. G. Brickwedde, National Bureau of Standards Paper No. RP1932, 1948.
[50]L. Haar, A. S. Friedman, and C. W. Beckett, *Ideal Gas Thermodynamic Functions and Isotope Exchange Functions for the Diatomic Hydrides, Deuterides, and Tritides*, National Bureau of Standards Monograph No. 20 (U.S. Government Printing Office, Washington, 1961).
[51]H. L. Johnston and E. A. Long, J. Chem. Phys. **2**, 389 (1934).
[52]R. Kosloff, R. D. Levine, and R. B. Bernstein, Mol. Phys. **27**, 981 (1974).
[53]E. W. Lemmon and M. O. McLinden, J. Chem. Eng. Data **54**, 3141 (2009).